ELSEVIER

Catalysis Today 44 (1998) 285–291

CATALYSIS TODAY

Investigation of redox potential and negative differential resistance behavior of heteropolyacids by scanning tunneling microscopy

In Kyu Song[a,*], Mahmoud S. Kaba[b], Mark A. Barteau[b], Wha Young Lee[c]

[a]*Department of Industrial Chemistry, Kangnung National University, Kangnung, Kangwondo 210-702, South Korea*
[b]*Department of Chemical Engineering, Center for Catalytic Science and Technology, University of Delaware, Newark, DE 19716, USA*
[c]*Department of Chemical Engineering, Seoul National University, Shinlim-dong, Kwanak-ku, Seoul 151-702, South Korea*

Abstract

Nanoscale images and tunneling spectra of cation-exchanged or polyatom-substituted heteropolyacids (HPAs) were probed by scanning tunneling microscopy (STM) at room temperature. All the HPAs formed two-dimensional ordered arrays on graphite surfaces, and their molecular dimensions were in good agreement with values determined by X-ray crystallography. It was observed that the negative differential resistance (NDR) peak voltage measured by STM was closely related to the reduction potential of the corresponding bulk HPA. The higher the reduction potential of the HPA, the lower the applied voltage at which NDR was observed.

Keywords: STM; NDR; Redox potential; Heteropolyacid

1. Introduction

Scanning tunneling microscopy (STM) allows surfaces to be imaged with angstrom scale resolution [1,2]. Although the emphasis of much early STM work was on the study of semiconductor surfaces [3], it has been used to image a variety of materials [4]. Many insulating materials such as proteins [5], liquid crystals [6], petroleum asphaltenes [7] and Langmuir–Blodgett films [8] have been successfully imaged using STM by depositing these materials on a conductive substrate. Several models [9,10] have been proposed to explain the significant tunneling current obtained through the electrically insulating sublayers of these systems. STM images of heteropoly and isopolyacids deposited on conductive substrates have been reported by several researchers [11–13]. Recent papers [14–16] reporting STM images of heteropolyacids (HPAs) showed that two-dimensional ordered arrays of these molecules on a graphite surface exhibited a distinctive current–voltage (I–V) behavior referred to as negative differential resistance (NDR) in their tunneling spectra. The observation of NDR features at spatially well-resolved positions in these arrays can be utilized to distinguish inequivalent sites and may be utilized to distinguish different polyoxometals in a mixed array. This may be a very important feature for the development of chemical sensors using HPAs for surface functionalization.

Heteropolyacids (HPAs) are inorganic acids as well as oxidizing agents [17–19]. They are highly soluble

*Corresponding author. Tel.: 82 391 640 2404; fax: 82 391 640 2244; e-mail: inksong@knusun.kangnung.ac.kr

0920-5861/98/$32.00
PII S0920-5861(98)00201-6

in polar solvents such as water, alcohols and amines, but some HPAs are insoluble in non-polar chemicals such as benzene and olefins [20–22]. The solubility of HPAs in turn is closely related to their ability to adsorb reactants. Polar substances readily penetrate into the bulk of HPAs to form a pseudo-liquid phase [23,24], whereas non-polar chemicals are mostly adsorbed on the surface of HPAs [25]. Owing to these characteristics, HPAs have been widely investigated and have been used in a commercial process producing methacrylic acid [26]. It is well known [27–29] that the acid and redox properties of HPA can be controlled in a systematic way by replacing the protons with metal cations and/or by changing the heteroatom or the framework transition-metal atoms.

The size of $PMo_{12}O_{40}^{3-}$, the typical Keggin-type [30] heteropolyanion, is ca. 10–12 Å as determined by X-ray crystallography [31]. Fig. 1 shows a polyhedral representation of the molecular structure of the Keggin-type heteropolyanion of $PMo_{12}O_{40}^{3-}$ [32]. The structure of $PMo_{12}O_{40}^{3-}$ consists of a heteroatom, P, at the center of the anion cluster, tetrahedrally coordinated to four oxygen atoms. This tetrahedron is surrounded by 12 MoO_6 octahedra.

In this work, 12-heteropoly compounds were prepared and deposited on a highly oriented pyrolytic graphite (HOPG) surface to obtain images and tunneling spectra at room temperature. The observed NDR peak voltages of HPA monolayers were correlated with redox potentials of bulk HPAs with variation of counter cations and framework atoms. This is a typical example showing how we can relate the bulk properties of HPAs to surface properties of nanostructured HPA monolayers determined by STM.

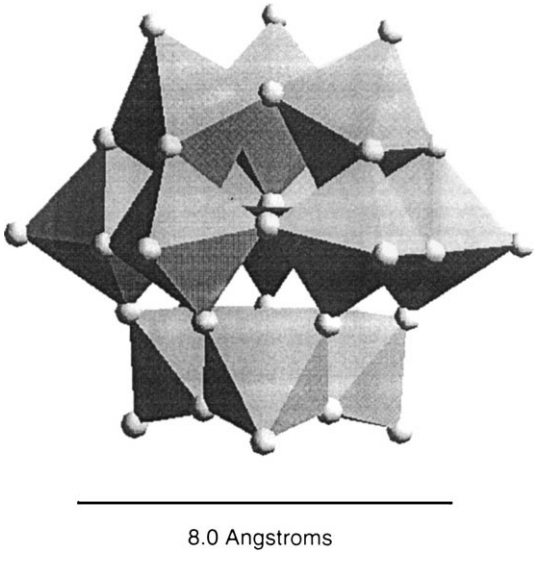

Fig. 1. Polyhedral representation of the molecular structure of $PMo_{12}O_{40}^{3-}$ [32].

2. Experimental

2.1. HPA deposition

$H_3PMo_{12}O_{40}$ was obtained from Aldrich. It was recrystallized from water and calcined at 300°C for precise quantification. Cation-exchanged $H_{3-x}Cs_xMo_{12}O_{40}$ (x=0–3) and $H_{3-x}Cu_{x/2}PMo_{12}O_{40}$ (x=0–3) were prepared as described elsewhere [33]. Polyatom-substituted $H_3PMo_{12-x}W_xO_{40}$ (x=0–12) was prepared according to a method in a literature [32] and $H_{3+x}PMo_{12-x}V_xO_{40}$ (x=0–3) was kindly supplied by the DuPont. Approximately 0.01 M aqueous solutions of each sample were prepared. A drop of each solution was deposited on freshly cleaved HOPG surface and allowed to dry in air at room temperature.

2.2. STM image and tunneling spectrum

STM images were obtained in air using a Topometrix STM (Discoverer). Mechanically formed Pt/Ir tips were used. Scanning was done in the constant current mode at a positive sample bias of 100 mV and tunneling current of 1–2 nA. Tunneling spectra were measured in air. Both Topometrix STM and LK Technologies STM (LK-1000) were used to perform consistent and reproducible tunneling spectroscopy. All the STM images presented in this paper are unfiltered, and the reported periodicities are average values determined by performing fast Fourier transform (FFT) analyzes on at least three images for each sample. To measure a tunneling spectrum, the sample bias was ramped from −2 to +2 V with respect to the tip, and the tunneling current was monitored. The voltage axis in the tunneling spectrum represents the potential applied to the sample relative to that of the tip.

2.3. Measurement of redox potential

The reduction potential of $H_3PMo_{12}O_{40}$ was measured gravimetrically using a Cahn 2000 electrobalance. About 50 mg of HPA sample was placed into the electrobalance and evacuated at room temperature. And then helium (80 cm^3/min) was continuously supplied to the balance as a carrier gas. The balance was maintained at 330°C for 3 h in order for the instrument to stabilize before the reduction process. Hydrogen was allowed to flow through the balance at the rate of 50 cm^3/min to begin the reduction process at 330°C. The weight loss of HPA sample was continuously monitored with reduction time until there was no change in the weight. The reduction potential of HPA sample was presented as the number of oxygen loss per heteropolyanion.

3. Results and discussion

3.1. Self-assembled and well-ordered HPA arrays

Fig. 2 shows the STM image of $H_3PMo_{12}O_{40}$ and $H_3PW_{12}O_{40}$ deposited on HOPG. Images of HOPG having periodicities of 2.46 Å and exhibiting its characteristic tunneling spectrum were also obtained prior to acquiring the STM images of HPAs. This was the standard calibration procedure to test the quality of Pt/Ir tips in our STM measurements. STM images in Fig. 2 clearly indicate the formation of self-assembled and well-ordered HPA arrays on HOPG. The periodicities of $H_3PMo_{12}O_{40}$ and $H_3PW_{12}O_{40}$ are 10.77±0.26 Å and 11.66±0.25 Å, respectively, and these values are in good agreement with molecular dimensions of Keggin-type HPAs determined by X-ray crystallography [31]. The unit cells constructed on the basis of lattice constant determined from two-dimensional FFT show that $H_3PMo_{12}O_{40}$ and $H_3PW_{12}O_{40}$ arrays possess nearly square symmetry (α=84.9° and α=79.5°, respectively).

3.2. NDR observation and monolayer confirmation

There is no particular reason to expect strong chemical and electronic interactions between HPA molecules and the HOPG surface in this system. Indeed, the formation of two-dimensional ordered arrays with periodicities unrelated to that of the chemically inert HOPG argues against binding at specific surface sites and against strong surface-adsorbate interaction.

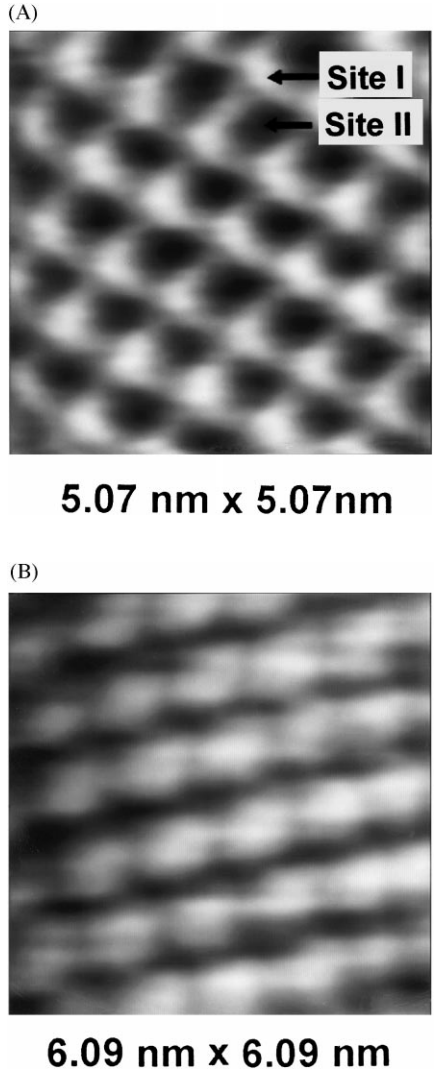

Fig. 2. STM image of (a) $H_3PMo_{12}O_{40}$ and (b) $H_3PW_{12}O_{40}$.

I–V spectra of $H_3PMo_{12}O_{40}$ arrays on HOPG taken at two different sites, denoted as site I and site II in Fig. 2(a), are shown in Fig. 3(a). Site II exhibits the typical I–V spectrum of graphite and site I exhibits the characteristic I–V spectrum of $H_3PMo_{12}O_{40}$. Site I in Fig. 2(a) shows a negative differential resistance (NDR) behavior where dI/dV is negative in some region as shown in Fig. 3(b). The NDR peak voltage

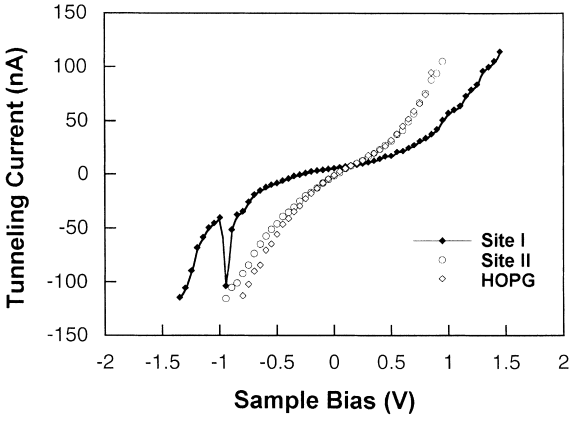

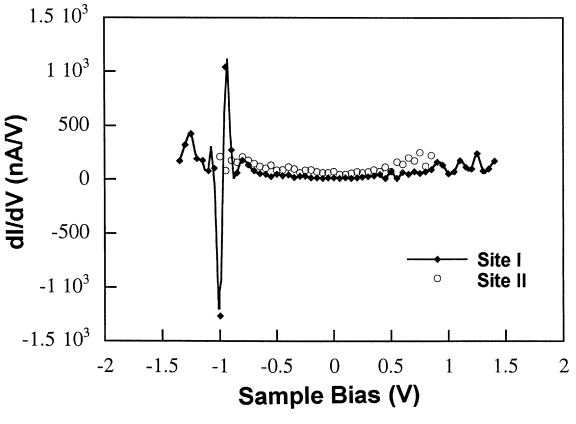

Fig. 3. I–V spectra taken at two different sites in Fig. 2(a): (a) I–V spectra and (b) dI/dV–V spectra.

is defined as the voltage where the maximum current is observed in this region. The NDR peak voltage of $H_3PMo_{12}O_{40}$ was determined to be −0.95 V. The difference in I–V spectra at the two sites, along with the observation of the characteristic I–V spectrum of graphite at the interstitial positions in the array, indicates that the two-dimensional ordered array is a monolayer, at least in the region of clear STM image. The striking NDR behavior of nanostructured HPA arrays measured by STM may be closely related to the electronic properties of these materials, and may serve as a fingerprint of their redox properties.

3.3. NDR behavior and reduction state

Fig. 4 illustrates the amount of oxygen removed from bulk sample of $H_3PMo_{12}O_{40}$ as a function of

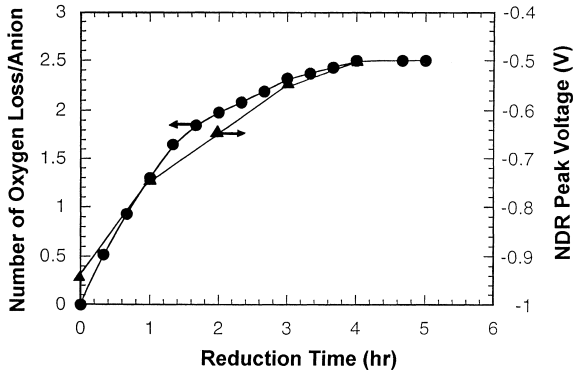

Fig. 4. Extent of reduction (●) and NDR peak voltage (▲) as a function of reduction time in H_2 at 330°C.

reduction time in H_2 at 330°C. Also shown is the NDR peak voltage measured for samples reduced for up to 4 h and then dispersed in monolayer arrays on graphite. Taking into account the resolution of the tunneling spectroscopy measurements (±0.05 V), the two curves are essentially superimposable. As the number of oxygen atoms removed per anion increases from 0 to 2.5, the NDR peak shifts from −0.95 to −0.5 V with the same transient behavior with respect to reduction time. This correspondence is illustrated further in Fig. 5, which demonstrates the linear relationship between the change in oxygen content and the shift in NDR peak voltage from the respective values for stoichiometric $H_3PMo_{12}O_{40}$. Such correlations demonstrate that NDR measurements on individual

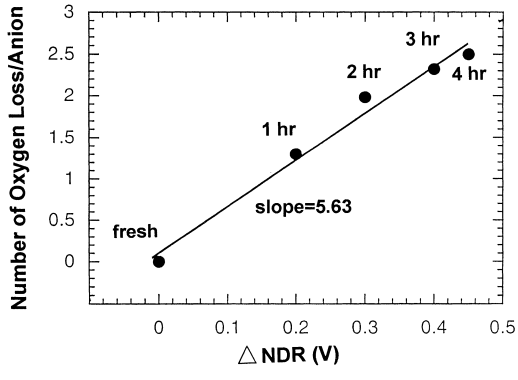

Fig. 5. Correlation between extent of reduction and NDR peak voltage shift for $H_3PMo_{12}O_{40}$; (△) NDR=I NDR(reduced)-NDR(fresh) I.

molecules in these monolayer arrays can be used to fingerprint their extent of reduction.

It is notable that NDR peak position moves toward less applied negative voltage when the HPA is reduced. The sample is biased positive while imaging. This means that electrons flow from tip to sample in the normal mode of operation whereas NDR behavior is observed in the tunneling spectra when electrons tunnel from sample to tip at negative applied voltage. It is believed that higher electron density of the reduced HPA leads to the appearance of NDR behavior at less negative applied voltage. It is clear that NDR behavior of nanostructured HPA arrays measured by STM is closely related with the electronic properties of bulk HPAs.

3.4. *Effect of counter cation*

Fig. 6 shows the correlation between NDR peak voltages measured with the STM [14] and the reciprocals of reduction temperature of cation-exchanged $H_3PMo_{12}O_{40}$ measured by Ai [34]. Replacement of a proton by a Cs cation decreases the reduction potential (increases the reduction temperature) of the HPA catalyst and shifts the NDR peak voltage to larger negative values in the tunneling spectrum. However, replacement of a proton by a Cu cation has the exact opposite effects on redox properties and on NDR behavior of the HPA catalyst. The reduction potential increases and the NDR peak voltage decreases in magnitude with increasing Cu content. It is concluded that more reducible HPAs show NDR behavior at less negative applied voltages.

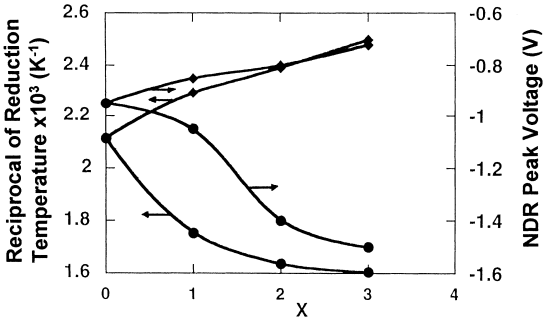

Fig. 6. A correlation between NDR peak voltage [14] and reduction potential [36] of $H_{3-x}Cs_xMo_{12}O_{40}$ (●) and $H_{3-x}Cu_{x/2}PMo_{12}O_{40}$ (◆).

A previous study [35] explaining the effects of counter cation on the redox properties of 12-molybdophosphates suggests that Cu ions gain more electrons than Cs ions during the reduction process. Since the electrons supplied to the sample by reduction are presumably distributed between heteropolyanion and counter cation, it has been suggested that Cu, which is more electronegative than Cs, acts as a large electron reservoir to facilitate electron transfer to the molybdenum ion in the reducing environment by providing a route for electron delocalization [35].

3.5. *Effect of framework substitution*

Fig. 7 shows the correlation between NDR peak voltages of $H_3PMo_{12-x}W_xO_{40}$ samples and their oxidation catalytic activity of CO reported in a literature [36]. It is well known that Mo-containing HPAs have greater redox potentials than W-containing HPAs. In other words, the reduction potential of $H_3PMo_{12-x}W_xO_{40}$ increases with the increase in the extent of Mo framework substitution. The NDR peak of $H_3PMo_{12-x}W_xO_{40}$ shifts to less negative applied voltages with the increase in Mo content. This trend is quite consistent with the results of Fig. 6 in that more reducible HPAs show NDR behavior at less negative applied voltages. This result is also well supported by the CO_2 yield resulting from the reduction of $H_3PMo_{12-x}W_xO_{40}$ by CO at 300°C as shown in Fig. 7.

Although the NDR voltages and redox potentials of $H_{3+x}PMo_{12-x}V_xO_{40}$ did not vary monotonously with framework substitution unlike $H_3PMo_{12-x}W_xO_{40}$, a

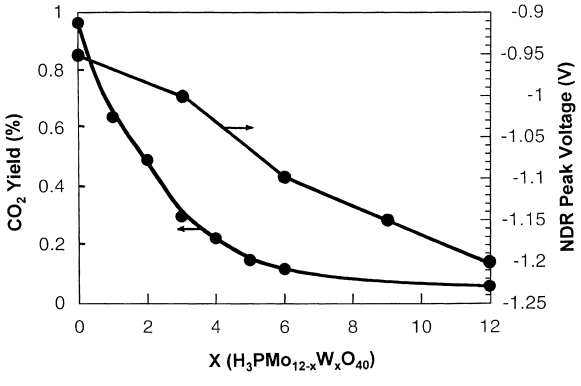

Fig. 7. Effect of framework substitution of $H_3PMo_{12-x}W_xO_{40}$ on NDR peak voltage and reduction potential [37].

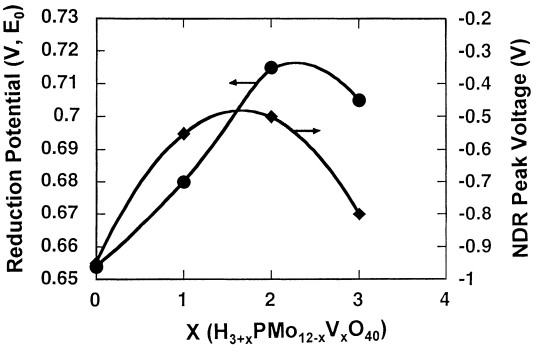

Fig. 8. Effect of framework substitution of $H_{3+x}PMo_{12-x}V_xO_{40}$ on NDR peak voltage and reduction potential [37].

good correlation between NDR peak voltages and reduction potentials was observed as shown in Fig. 8. The reduction potentials in Fig. 8 were taken from a literature [37], where the reduction potential was measured by electrochemical methods. The higher the E_0 value, the higher the reduction potential. $H_5PMo_{10}V_2O_{40}$ showed the highest reduction potential and the smallest negative NDR peak voltage among four HPAs. It is clear that NDR behavior of HPAs measured by STM can be a fingerprint of the redox potential of the bulk HPA. The above results imply that we can estimate the redox potential of bulk HPAs simply by measuring the NDR peak voltage of HPA arrays by STM. Thus, STM provides a tool for the characterization of bulk HPA catalysts through the characterization of nanostructured HPA monolayers.

4. Conclusions

STM images and tunneling spectra of cation-exchanged or framework-substituted $H_3PMo_{12}O_{40}$ were observed at room temperature. The HPAs formed self-assembled and well-ordered arrays on HOPG, and their periodicities were in good agreement with the molecular dimensions determined by X-ray crystallography. It was observed that the NDR peak voltage measured by STM was closely related to the reduction potential of bulk HPA assembly. The higher the reduction potential of the HPA, the lower the applied voltage at which NDR was observed. STM provided a strong tool for estimating the redox properties of bulk HPAs through the nanoscale characterization of HPA monolayers.

Acknowledgements

We acknowledge the support from Korea Research Foundation and National Science Foundation (CTS 9410965) for this work.

References

[1] G. Binnig, H. Rohrer, C. Gerber, E. Weibel, Phys. Rev. Lett. 49 (1982) 57.
[2] G. Binnig, H. Rohrer, Surf. Sci. 126 (1983) 236.
[3] T. Matsumoto, H. Tanaka, T. Kawai, S. Kawai, Surf. Sci. 278 (1992) L153.
[4] P.K. Hansma, J. Tersoff, J. Appl. Phys. 61 (1987) R1.
[5] L. Haggerty, B.A. Watson, M.A. Barteau, A.M. Lenhoff, J. Vac. Sci. Tech. B 9 (1991) 1219.
[6] W. Mizutani, M. Shigeno, M. Ono, K. Kajimura, Appl. Phys. Lett. 56 (1990) 1974.
[7] B.A. Watson, M.A. Barteau, Ind. Eng. Chem. Res. 33 (1994) 2358.
[8] B.H. Loo, Z.F. Liu, A. Fujishima, Surf. Sci. 227 (1990) 1.
[9] M.G. Youngquist, J.D. Baldeschwieler, J. Vac. Sci. Tech. B 9 (1991) 1083.
[10] G. Chen, G. Klimeck, S. Datta, G. Chen, W.A. Goddard, Phys. Rev. B 50 (1994) 8035.
[11] B. Keita, L. Nadjo, Surf. Sci. Lett. 254 (1991) L443.
[12] B.A. Watson, M.A. Barteau, L. Haggerty, A.M. Lenhoff, R.S. Weber, Langmuir 8 (1992) 1145.
[13] M. Ge, B. Zhong, W.G. Klemperer, A.A. Gewirth, J. Am. Chem. Soc. 118 (1996) 5812.
[14] M.S. Kaba, I.K. Song, M.A. Barteau, J. Phys. Chem. 100 (1996) 19577.
[15] I.K. Song, M.S. Kaba, M.A. Barteau, J. Phys. Chem. 100 (1996) 17528.
[16] I.K. Song, M.S. Kaba, G. Coulston, K. Kourtakis, M.A. Barteau, Chem. Mater. 8 (1996) 2352.
[17] I.K. Song, S.H. Moon, W.Y. Lee, Korean J. Chem. Eng. 8 (1991) 33.
[18] I.V. Kozhevnikov, Catal. Rev. Sci. Eng. 37 (1995) 311.
[19] T. Okuhara, N. Mizuno, M. Misono, Adv. Catal. 41 (1996) 113.
[20] I.V. Kozhevnikov, K.I. Matveev, Appl. Catal. 5 (1983) 135.
[21] M. Misono, Mater. Chem. Phys. 17 (1987) 103.
[22] N. Mizuno, M. Misono, Chem. Lett. (1984) 669.
[23] M. Misono, K. Sakata, Y. Yoneda, W.Y. Lee, in: T. Seiyama, K. Tanabe (Eds.), New Horizons in Catalysis, Proceedings of the Seventh International Congress on Catalysis, Tokyo, 30 June–4 July 1980, Studies on Surface Science Catalysis, vol. 7B, Kodansha, Tokyo, Elsevier, Amsterdam, 1980, p. 1047.

[24] K.Y. Lee, T. Arai, S. Nakata, S. Asaoka, T. Okuhara, M. Misono, J. Am. Chem. Soc. 114 (1992) 2836.
[25] M. Misono, Catal. -Rev. -Sci. Eng. 29 (1987) 269.
[26] Y. Konishi, K. Sakata, M. Misono, Y. Yoneda, J. Catal. 77 (1982) 169.
[27] N. Mizuno, M. Misono, J. Mol. Catal. 86 (1994) 319.
[28] H. Hayashi, J.B. Moffat, J. Catal. 81 (1983) 61.
[29] C.L. Hill, C.M. Prosser-McCartha, Coord. Chem. Rev. 143 (1995) 407.
[30] J.F. Keggin, Nature 131 (1933) 908.
[31] G.M. Brown, M.R. Noe-Spirlet, W.R. Busing, H.A. Levy, Acta. Cryst. B 33 (1977) 1038.
[32] M.T. Pope, Heteropoly and Isopoly Oxometalates, Springer, New York, 1983.
[33] G.A. Tsigdinos, Ind. Eng. Chem. Res. 13 (1974) 267.
[34] M. Ai, Appl. Catal. 4 (1982) 245.
[35] H.C. Kim, S.H. Moon, W.Y. Lee, Chem. Lett. (1991) 447.
[36] M. Akimoto, H. Ikeda, A. Okabe, E. Echigoya, J. Catal. 89 (1984) 196.
[37] I.V. Kozhevnikov, E.G. Zhizhina, N.B. Kuznetsova, Kinet. Katal. 56 (1987) 811.